Power management via STL specifications of a DC microgrid integrating renewables and storage devices: a smart railway station case study

Yoshinari Takayama, Adnane Saoud, Alessio Iovine

Power management via STL specifications of a DC microgrid integrating renewables and storage devices: a smart railway station case study

Yoshinari Takayama [*] **Adnane Saoud** [**,*] **Alessio Iovine** [*]

[*] *Laboratory of Signals and Systems (L2S), CNRS, CentraleSupelec, Paris-Saclay University 3, rue Joliot Curie, 91190 Gif-sur-Yvette, France* {*name.surname*}*@centralesupelec.fr*
[**] *College of Computing, University Mohammed VI Polytechnic, Benguerir, Morocco adnane.saoud@um6p.ma*

Abstract: This paper presents a method for defining and managing complex power management behaviors in microgrids that incorporate renewable energy sources, storage devices with different characteristics, and a connection to the main grid. In particular, we focus on a smart railway station that integrates regenerative braking energy from trains. The challenge lies in coordinating diverse microgrid components while adhering to constraints across multiple control levels. We use signal temporal logic (STL) to precisely define these complex objectives and integrate them into a model predictive control (MPC) framework. We present numerical simulations using a mixed-integer strategy to demonstrate the approach's effectiveness.

Keywords: power management, signal temporal logic, model predictive control, railway station

1. INTRODUCTION

The increasing complexity of power systems, with their numerous physical and cyber components, makes it difficult to define comprehensive specifications for managing interactions across control levels (see Derler et al. (2012); Nuzzo et al. (2014); Taousser et al. (2020)). This challenge is amplified in microgrids, which offer fewer degrees of freedom and a smaller stability region with respect to bulk power systems. In this paper, we focus on defining temporal specifications for power management within a Direct Current (DC) microgrid tailored for a smart railway station. Our goals are to recover regenerative braking energy for enhanced efficiency (see Scheepmaker and Goverde (2020); Feng et al. (2021)) and to improve air quality by minimizing mechanical brake usage (see González-Gil et al. (2013)). However, integrating this capability increases grid instability, potentially compromising power quality and necessitating stricter grid code compliance (see Araúz and Martinez (2023)).

To address these complexities, the microgrid requires appropriately sized storage components. A combination of a battery for sustained power delivery and a supercapacitor for rapid responses, that is, a hybrid storage system, is crucial (see Sheng et al. (2019)). A hierarchical control approach is promising for effective management of these multi-component microgrids. Coordination among components and layers is necessary to achieve desired behaviors (see Iovine et al. (2019)). This includes maintaining an optimal State-of-Charge (SoC) for the supercapacitor and ensuring appropriate power quality for the Alternate Current (AC) grid connection. In scenarios where the battery SoC approaches its limit, we might prioritize accommodating an incoming train's regenerative power by preemptively pausing battery charging. This optimal coordination within the secondary level necessitates understanding how specifications impact primary-level actions, including potential limitations when modeling across time scales. Furthermore, constraints, such as economic agreements with the AC grid, might change over time when we consider the tertiary level. These changes must be clearly communicated to the secondary level using a standardized mathematical language.

To define these desired behaviors of interactions between layers and components, we employ signal temporal logic (STL) with quantitative semantics. Temporal logic is promising (e.g., Xu et al. (2018); Taousser et al. (2020); Wooding et al. (2020); Liu et al. (2022)) as it translates natural language specifications into mathematical forms for analyzing temporal dynamics in systems. These representations can be automatically transformed into decision problem constraints using available tools (e.g., Donzé and Raman (2015); Kurtz and Lin (2022); Takayama et al. (2023a,b)), simplifying implementation for engineers. STL's inclusion via binary variables leads to a mixed-integer optimization problem (see Raman et al. (2014); Park and Olama (2021)). Compared to traditional rule-based constraints (e.g., Pham et al. (2022)), STL offers a more rigorous and expressive way to define requirements.

[1] This work has received funding from the Agence Nationale de la Recherche (ANR) via grant ESTHER ANR-22-CE05-0016. Y. Takayama acknowledges the support of the Watanabe Foundation International Fellowship.

This paper focuses on using STL at the secondary control level considering the interactions between diverse components within a microgrid. In contrast to previous work on model predictive control (MPC) for the secondary layer without STL formulations (e.g., Sheng et al. (2019); Iovine et al. (2019)), we leverage STL's expressiveness to achieve more detailed requirements, rather than simply pursuing the classical objectives, such as stability and safety. Moreover, this application of STL, considering interactions between layers in the secondary control, is relatively new compared to its use purely for primary-level frequency support or bulk system storage, e.g., Beg et al. (2019); Xu et al. (2019).

This paper is organized as follows. Section 2 presents the DC microgrid model and outlines the control objectives. Section 3 introduces STL and demonstrates how we use it to formalize control goals. These goals include adjusting AC grid power flow upon train arrival, strategically limiting battery charging to absorb train power later, and defining operational regions for the supercapacitor (discussed in Subsections 3.2–3.4). Subsection 3.5 then presents the formulation of our optimization problem. Finally, Section 4 provides numerical results to illustrate the effectiveness of our approach.

2. MODELING AND CONTROL APPROACH

Notation Let $\mathbb{R}$, $\mathbb{N}$, and $\mathbb{N}_{>0}$ be the set of real numbers, integers, and positive integers, respectively. For $x \in \mathbb{R}$, $|x|$ denotes its absolute value.

2.1 Microgrid Model

Our focus in this paper is the secondary control layer in connection with the layers above and below in Fig. 1, which is in charge of managing powers and energies for power balance purposes. Section 2.4 gives a more detailed explanation of this hierarchical structure. In this secondary layer, stored energy levels in the DC microgrid, battery, and supercapacitor are influenced by the interaction between PV generation, regenerative braking, the AC grid, and load demand. Energy variations within the battery and supercapacitor depend directly on their power output. In contrast, DC microgrid energy changes are determined by the overall power balance between generation and consumption. Specifically, the power flow dynamics of the considered microgrid are (see Sheng et al. (2019)):

$$
\begin{cases}
E_{DC}(k+1) = E_{DC}(k) - T[\frac{1}{\eta_L}(D_L(k) - P_L(k))] \\
+T[\eta_{PV}(D_{PV}(k) - P_{PV}(k)) + \eta_B^+ P_B^+(k)] + \\
+T\left[-\frac{1}{\eta_B^-}P_B^-(k) + \eta_S^+ P_S^+(k) - \frac{1}{\eta_S^-}P_S^-(k)\right] + \\
+T\left[\eta_T(D_T(k) - P_T(k)) + \eta_{AC}^+ P_{AC}^+(k) - \frac{1}{\eta_{AC}^-}P_{AC}^-(k)\right] \\
E_B(k+1) = E_B(k) \ + T\left[P_B^-(k) - P_B^+(k)\right] \\
E_S(k+1) = (1 - T\alpha_S)E_S(k) \\
\qquad\qquad +T\left[P_S^-(k) - P_S^+(k)\right] + w(k),
\end{cases}
$$

where $E_B, E_S, E_{DC} \in \mathbb{R}$ are the energies stored in the battery, supercapacitor, and microgrid, respectively. $D_{PV} - P_{PV}$ is the power produced by the PV array, where $D_{PV} \in \mathbb{R}$ is the current available power and $P_{PV} \in \mathbb{R}$ is the amount of power to be cut off for the stability of the entire grid; according to the same reasoning, $D_L - P_L$ is the power demanded by the load, with $D_L \in \mathbb{R}$ the current demanded power and $P_L \in \mathbb{R}$ the amount of power to be curtailed. With similar configuration, $D_T - P_T$ is the power produced by the train braking, where $D_T \in \mathbb{R}$ is the current available power and $P_T \in \mathbb{R}$ is the neglected one. The incorporation of P_{PV}, P_L, and P_T is motivated by the imperative to ensure the existence of optimal solutions. This is particularly crucial in scenarios where an excess of power is injected into the microgrid, as seen with D_{PV} or D_T, which can be mitigated through adjustments in P_{PV} or P_T, or when the supplied power falls short of meeting the demand, as indicated by P_L reducing D_L. P_B^+, P_B^-, P_S^+, P_S^-, P_{AC}^+, $P_{AC}^- \in \mathbb{R}$ are the powers exchanged by the battery,the supercapacitor, and the AC grid, respectively, where P_B^+, P_S^+, P_{AC}^+ are the provided powers and P_B^-, P_S^-, P_{AC}^- are the absorbed ones. We introduced distinct variables for charging and discharging to consider the losses stemming from the physical characteristics, which may lead to different values in the charge and discharge scenarios. The parameters η_{PV}, $\frac{1}{\eta_L}$, η_B^d, $\frac{1}{\eta_B^c}$, η_S^d, $\frac{1}{\eta_S^c}$, η_{AC}^+, $\frac{1}{\eta_{AC}^-} \in \mathbb{R}$ describe the loss in efficiency due to $D_{PV} - P_{PV}$, $D_L - P_L$, P_B^+, P_B^-, P_S^+, P_S^-, P_A^+, P_A^-, respectively. A parameter α_S is introduced to account for the self-discharge ratio of the supercapacitor within the specified time interval T; the negligible self-discharge ratio of the battery is disregarded due to the relatively short time span considered in relation to the battery dynamics.

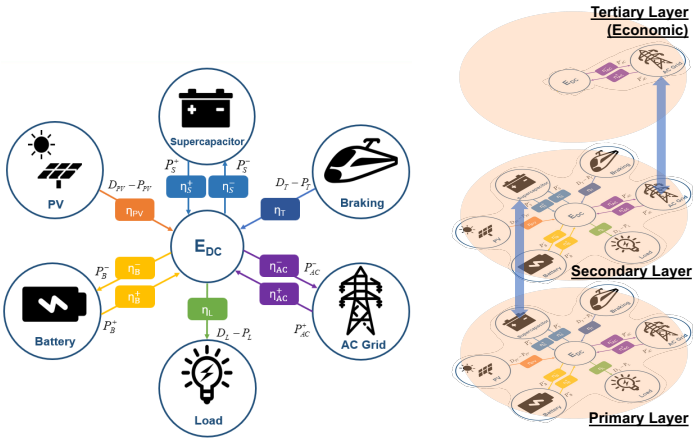

(a) The microgrid (b) Layers

Fig. 1. (a) The considered microgrid and (b) the three layers of the proposed control approach. The supercapacitor is in charge of connecting the primary and the secondary layers, while the AC grid connects the tertiary and the secondary layers. Details of (b) are in Section 3.

The system results in a linear system of the form:

$$x(k+1) = Ax(k) + Bu(k) + Dd(k) + Ww(k) \qquad (1)$$

where the state x, the control input u, the disturbance w, and the discrete-time matrices $A, B = [\,B_1 \ B_2\,], D, W$ are

$$x = [E_{DC}\ E_B\ E_S]^\mathsf{T}, d = [D_{PV}\ D_L\ D_T]^\mathsf{T},$$
$$u = \left[P_{PV}\ P_L\ P_B^+\ P_B^-\ P_S^+\ P_S^-\ P_T\ P_{AC}^+\ P_{AC}^-\right]^\mathsf{T},$$

$$A = \begin{bmatrix} 1 & 0 & 0 \\ 0 & 1 & 0 \\ 0 & 0 & 1 - T\alpha_S \end{bmatrix}, \quad D = \begin{bmatrix} \eta_{PV} & -\frac{1}{\eta_L} & \eta_T \\ 0 & 0 & 0 \\ 0 & 0 & 0 \end{bmatrix},$$

$$W = \begin{bmatrix} 0 \\ 0 \\ 1 \end{bmatrix}, \quad B_1 = \begin{bmatrix} -\eta_{PV} & \frac{1}{\eta_L} & \eta_B & -\frac{1}{\eta_B} \\ 0 & 0 & -1 & 1 \\ 0 & 0 & 0 & 0 \end{bmatrix},$$

$$B_2 = \begin{bmatrix} \eta_S & -\frac{1}{\eta_S} & -\eta_T & \eta_{AC} & -\frac{1}{\eta_{AC}} \\ 0 & 0 & 0 & 0 & 0 \\ -1 & 1 & 0 & 0 & 0 \end{bmatrix},$$

and $w(k)$ is a Gaussian disturbance with the variance being 0.01, i.e., $w(k) \sim \mathcal{N}(0, 0.01)$.

It is worth noting that we add a disturbance solely to the supercapacitor component in our hierarchical control scheme, differently from Iovine et al. (2019). This reflects the fact this primary-secondary layer mismatch most impacts the supercapacitor. By introducing the noise, we can avoid detailed modeling of primary-level currents and voltages dynamics (see Perez et al. (2020) for more details). A complete model would use real-time measurements to reconcile differences between the layers, where the secondary layer provides the references to components. In contrast, a lower primary layer generates high-frequency control inputs based on those references. However, our current model cannot account for the fast variations handled by the primary layer, leading to a mismatch between the desired supercapacitor state and its actual state. Without this disturbance, the computed optimal solutions would unrealistically assume perfect supercapacitor tracking.

2.2 Constraints

To protect the physical devices, the state variables representing the energy are constrained between a minimum and a maximum level, i.e., $E_{DC}^m \leq E_{DC}(k) \leq E_{DC}^M, E_B^m \leq E_B(k) \leq E_B^M, E_S^m \leq E_S(k) \leq E_S^M, \forall k$, where $E_{DC}^m, E_{DC}^M > 0$ are needed to ensure power quality and to avoid problems related to the connection with the physical devices, and $E_B^m, E_B^M > 0$ and $E_S^m, E_S^M > 0$ define the safe range of values for the storage devices. Clearly, due to the sizes of the devices, it results in $E_{DC}^M << E_S^m < E_B^m$. Let us mention that we chose to model the DC microgrid as a state variable instead of just describing its dynamics as a constraint for a matter of generality. This allows for considering a storage device playing the role of the DC bus, if needed by the application.

To accurately represent different efficiencies during the charging and discharging phases, we use two separate variables for power output. This approach is necessary, as storage devices cannot simultaneously charge and discharge (see Parisio et al. (2014) for details). Therefore, the power absorbed/provided by storage devices must ensure that one of the variables is always zero:

$$0 \leq P_B^+(k) \leq S_B(k) \cdot \overline{P}_B^+, \forall k \tag{2a}$$
$$0 \leq P_B^-(k) \leq (1 - S_B(k)) \cdot \overline{P}_B^-, \forall k \tag{2b}$$
$$0 \leq P_S^+(k) \leq S_S(k) \cdot \overline{P}_S^+, \forall k \tag{2c}$$
$$0 \leq P_S^-(k) \leq (1 - S_S(k)) \cdot \overline{P}_S^-, \forall k \tag{2d}$$

where $\overline{P}_B^+, \overline{P}_B^- > 0$ and $\overline{P}_S^+, \overline{P}_S^- > 0$ are maximum values, and $S_B(k), S_S(k) \in \{0, 1\}$, for all k, are binary variable modeling the conditions $P_B^+(k) \times P_B^-(k) = 0$, for all k and $P_S^+(k) \times P_S^-(k) = 0$, for all k, respectively. These constraints can be formalized in terms of a mixed integer optimization problem.

As the lifetime of the battery is very important, hard constraints on battery power variation are imposed:

$$\left\| P_B^+(k+1) - P_B^+(k) \right\| \leq \Delta\overline{P}_B^+, \forall k \tag{3a}$$
$$\left\| P_B^-(k+1) - P_B^-(k) \right\| \leq \Delta\overline{P}_B^-, \forall k \tag{3b}$$

where $\Delta\overline{P}_B^+, \Delta\overline{P}_B^- > 0$. We do not impose similar constraints on the supercapacitor since it has to ensure voltage stability with respect to the fast variations acting on the grid.

Similarly to the constraints for storage devices and battery (2) and (3), the constraints for the connection with the AC grid are:

$$0 \leq P_{AC}^+(k) \leq S_{AC}(k) \cdot \overline{P}_{AC}^+, \forall k \tag{4a}$$
$$0 \leq P_{AC}^-(k) \leq (1 - S_{AC}(k)) \cdot \overline{P}_{AC}^-, \forall k \tag{4b}$$
$$\left\| P_{AC}^+(k+1) - P_{AC}^+(k) \right\| \leq \Delta\overline{P}_{AC}^+, \forall k \tag{4c}$$
$$\left\| P_{AC}^-(k+1) - P_{AC}^-(k) \right\| \leq \Delta\overline{P}_{AC}^-, \forall k \tag{4d}$$

where $\Delta\overline{P}_{AC}^+, \Delta\overline{P}_{AC}^- > 0$, $\overline{P}_{AC}^+, \overline{P}_{AC}^- > 0$ and $S_{AC}(k) \in \{0, 1\}$, for all k.

Finally, according to the signs depicted in Fig. 1a and the hypothesis that $D_{PV}(k) \geq 0$, $D_L(k) \geq 0$, $D_T(k) \geq 0$, for all k, we define the constraints that the supply power from renewables and the train, or demand by the load cannot be negative, i.e., the curtailment is constrained by $P_{PV}(k) \geq 0, P_L(k) \geq 0, P_T(k) \geq 0, D_{PV}(k) - P_{PV}(k) \geq 0, D_L(k) - P_L(k) \geq 0, D_T(k) - P_T(k) \geq 0, \forall k$.

2.3 Horizon Lengths for Prediction and Estimation

The proposed approach includes two parts: an MPC controller and an estimator for exogenous inputs (e.g., train power generation). We use different prediction horizons for the controller (N_p) and the estimator (N_e) to reflect real-world conditions. A smaller N_p is typical, particularly for complex systems and specifications, as this reduces computational complexity related to implementing STL specifications. We set $N_p = 10$. In contrast, we can use a longer estimation horizon ($N_e \geq N_p$), leveraging sensors for train detection. We set $N_e = 20$.

The estimator uses sensor data to predict the train's braking power trajectory. At each timestep k_c, the braking power estimation, denoted as $D_T(k_c : k_c + N_e - 1)$, is generated. This predicted braking power trajectory, along with estimations of other external inputs $D_{PV}(k_c : k_c + N_e - 1)$ and $D_L(k_c : k_c + N_e - 1)$, is provided to the predictive controller. Let us denote these estimated data of D_T, D_{PV}, D_L over the horizon N_e computed at sampling instant k_c as $\widetilde{\boldsymbol{d}} = (\widetilde{d}(0|k_c), \ldots, \widetilde{d}(N_e - 1|k_c))$. To simplify the notation, we will use $\widetilde{d}(k)$ to represent $\widetilde{d}(k|k_c)$ and $D_T(k)$ to represent $D_T(K_c + k)$. This applies similarly to other variables like $u(k)$ and $x(k)$.

In the classical MPC formulation, the additional estimation data outside the prediction horizon, i.e., the data of $D_T(N_p - 1 : N_e - 1)$, at each timestep k_c was not exploited. However, leveraging this data can significantly enhance the controller, particularly in our scenario where the train involves a sudden increase in power to over 1500 (kw) for 20 seconds before rapidly returning to 0 (kw) (see the orange line in Fig. 4). This sudden power generation can potentially overload the grid and strongly impact its stability. The predictive controller utilizes prior knowledge of the abrupt incoming power from the train braking through STL specifications.

2.4 Control Goals

The objective of this section is to describe, in an informal way, the considered control objectives in this paper. A formal description of the objectives in terms of STL will be considered in Section 3.

The overarching goal of this problem is to ensure power balance within the DC microgrid, along with tracking a desired energy reference (E^r_{DC}). Our first priority is minimizing load curtailment ($P^r_L = 0$ KW). Next, we aim to track a desired energy reference for the supercapacitor (E^r_S) to compensate for fast variations. We also prioritize minimizing the curtailment of generated power from PV and trains, followed by optimizing our interaction with the AC grid.

The DC microgrid will participate in the ancillary services market of the AC grid, adhering to a power reference ($P^r_{AC} = 200$ KW) determined by tertiary-level economic optimization based on market prices. This reference is generally followed but can be temporarily relaxed to prioritize train arrivals. Specification **Spec 1** models this strategic decision.

We aim to maximize renewable power generation and stored energy in the battery, aiming for a battery energy level near its maximum value (we chose $E^r_B = E_{BM} - 1.0 =$ 309.0 KWh to avoid the overload by the disturbance). This is guided by reference curtailment values for the PV and the train ($P^r_{PV} = 0$ KW, $P^r_T = 0$ KW). We prefer to curtail PV power due to its smoother nature, which also benefits air quality in the railway station. However, when a train is expected, we might limit battery charging, even if it is below the maximum capacity, to ensure it can absorb the train's regenerative braking power (**Spec 2**).

In practice, perfect control of the supercapacitor's energy level is difficult due to limitations in how the primary control layer tracks the reference value $P_S(k) = P^+_S(k) - P^-_S(k)$. The only available means to keep the supercapacitor's energy within safe bounds against the added disturbance is by controlling the power input/output of the battery, expressed as $P_B(k) = P^+_B(k) - P^-_B(k)$, which has a larger capacity. This input/output of the battery is determined by the requirements for DC grid balance taking other minor factors into account. In Section 3, we incorporate specification **Spec 3** to enhance the safety of the expected behavior of the supercapacitor. The formalization of these objectives **Spec 1**–**Spec 3** in terms of STL specifications will be considered in Subsections 3.2-3.4, respectively.

On the other hand, the aforementioned classical tracking control goals are modeled by the following quadratic cost function: $J = \frac{1}{2}\left[\tilde{x_N}^\mathsf{T} R \tilde{x_N} + \sum_{i=0}^{N_p-1} \tilde{x_i}^\mathsf{T} Q \tilde{x_i} + u_i^\mathsf{T} R u_i)\right]$, where $\tilde{x_t} = x_t - x^{\text{ref}}_t$, and $x^{\text{ref}}_t = [E^r_{DC}, E^r_B, E^r_S] = [1.39e^{-5}, 309, 4.5]^\mathsf{T}$. Regarding the u^{ref}_t, we also require each element of the control inputs u_t to track 0, except for P^-_{AC}, which is required to be $P^{-r}_{AC} = 200$ KW. This is because we want the reference $P^r_{AC} = P^{+r}_{AC} - P^{-r}_{AC} = -200$ KW. The weight matrix is $Q = [1e^{17}, 1e^9, 1e^{10}]^\mathsf{T}$ and $R = [5e^6, 1e^8, 5e^2, 5e^2, 1, 1, 5e^7, 1e^5, 1e^5]^\mathsf{T}$, where a relatively high weight is set to the objectives of P_{PV} and P_L as in practice, we prefer to charge or discharge the power to curtail the supply and the demand. The initial values for the state and the control are taken as $x_0 = [1.39e^{-5}, 306, 5.5]^\mathsf{T}$ and $u_0 = [0, 0, 0, 0, 0, 340, 0, 0, 200]^\mathsf{T}$.

3. STL SPECIFICATIONS

3.1 Signal Temporal Logic (STL)

We first provide a quick review of STL formalism. STL is a predicate logic that specifies continuous signal properties (see Fainekos and Pappas (2009)). Predicates, or atomic propositions, are a part of STL and take either True (1 or $\top$) or False (0 or $\bot$). In addition to the standard boolean operators $\wedge$ and $\vee$, the STL also incorporates temporal operators $\Box$ (*always*), $\Diamond$ (*eventually*), and $\boldsymbol{U}$ (*until*). The semantics of STL is defined as (Baier and Katoen (2008)):

$$\varphi := \mu | \neg\varphi | \vee \varphi | \wedge \varphi | \bigcirc \varphi | \Box_{[k_1,k_2]}\varphi | \Diamond_{[k_1,k_2]}\varphi \mid \varphi_1 \boldsymbol{U}_{[k_1,k_2]}\varphi_2, \tag{5}$$

where $\mu = (g^\mu(x_t) \leq 0), g^\mu : \mathbb{R}^n \to \mathbb{R}$ is a predicate, and the symbol | stands for OR and the definition is recursive. Each temporal operator has associated bounded time interval $[k_1, k_2]$ where $0 \leq k_1 < k_2$ and $k_2 < \infty$. For specifications $\varphi_1; \varphi_2$, the logical operator $\phi_1 \vee \phi_2$ is satisfied at time k if φ_1 and φ_2 are True at time k, and the logical operator $\phi_1 \wedge \phi_2$ is satisfied at time k if φ_1 or φ_2 are True at time k. The operator next $\bigcirc\varphi$ is satisfied at time k if φ is True at time $k+1$. The temporal operator always $\Box_{[k_1,k_2]}\varphi$ is satisfied at time k if φ is True at all times in $k + [k_1, k_2]$. The eventually operator $\Diamond_{[k_1,k_2]}\varphi$ is satisfied at time k if φ is True at some time in $k + [k_1, k_2]$. The temporal operator until $\varphi_1 \boldsymbol{U}_{[k_1,k_2]}\varphi_2$ is satisfied at time k if φ_2 is True at some time $k_3 \in [k+k_1, k+k_2]$ and such that φ_1 is True for all time in $[k, k_3]$. As an instance, formula $\varphi = \Box_{[0,2]}(x(k) > 0)$ evaluated at time 0 specifies that for all times between 0 and 2, $x(k) > 0$ is satisfied, the formula $\varphi = \Diamond_{[0,2]}(x(k) > 0)$ evaluated at time 0 specifies that there exists a time instant k between 0 and 2 such that $x(k) > 0$.

*3.2 **Spec 1:** Power Exchange with the Main Grid*

The first STL specification, **Spec 1**, implements a strategy for power exchange with the main AC grid. This strategy is determined at the tertiary level based on economic evaluations of the DC grid's potential to provide ancillary services. Due to the potential negative impacts of regenerative braking on the microgrid's stability and storage devices' state of health (SoH), we prioritize power quality by closely tracking a desired power reference. The only

exception is a short period around the train's braking: from 10 seconds before the estimated start of braking until 10 seconds after the braking ends. This strategic choice, determined at the tertiary level, is implemented through a specification:

$$\varphi_{\text{Tb}} = [D_T(k) \geq 1500], \tag{6}$$

$$\varphi_{\text{AC}} = [(P^-_{AC}(k) = 200) \wedge (P^+_{AC}(k) = 0)], \tag{7}$$

$$\varphi_{\text{Spec1}} = [(\Box_{[-10,10]} \neg \varphi_{\text{Tb}}) \rightarrow \varphi_{\text{AC}}], \tag{8}$$

$$\tilde{\varphi}_{\text{Spec1}} = \Box_{[0,N_p-1]} \varphi_{\text{Spec1}}. \tag{9}$$

Intuitively, φ_{Tb} is true when the train is braking at the prediction horizon k while φ_{AC} results in following the reference $P^r_{AC} = -200.0$ KW, because of the equation $P_{AC} = P^+_{AC} - P^-_{AC}$. Note that the specification φ_{Spec1} allows the microgrid to deviate from the power reference P^r_{AC} only for the emergency duration of the sudden incoming power, that is, when $\Box_{[-10,10]}\varphi_{\text{Tb}}$ is True. $\tilde{\varphi}_{\text{Spec1}}$ enforces φ_{Spec1} for all the prediction steps till $N_p - 1$.

3.3 ***Spec 2:*** *Preventive Halting of Battery Charging*

The second specification **Spec 2** concerns the battery, and more specifically aims to avoid critical situations where the energy is too close to the maximum level but a train arrival is foreseen. Classically, when the regenerative braking that cannot be stored in the microgrid comes, it is sent to the AC grid to avoid causing instability in the DC microgrid. However, this is not an option here, due to the willingness in the tertiary layer to limit variations from the reference value as described in Subsection 3.2.

To stabilize the entire grid without directing the entire generation from the train braking to the AC grid, we restrict the battery power output to only discharge mode just before the braking. We express this constraint through the following STL specification:

$$\varphi_{\text{Tbs}} = [\Diamond_{[0,20]}(\varphi_{\text{Tb}} \wedge \bigcirc \neg \varphi_{\text{Tb}})], \tag{10}$$

$$\varphi_{\text{Sref}} = [E^r_S - E_S(k) \leq 0], \quad \varphi_{\text{PBm}} = [P^-_B(k) = 0], \tag{11}$$

$$\varphi_{\text{Spec2}} = [(\varphi_{\text{Tbs}} \wedge \varphi_{\text{Sref}}) \rightarrow \varphi_{\text{PBm}}], \tag{12}$$

$$\tilde{\varphi}_{\text{Spec2}} = \Box_{[0,N_p-1]} \varphi_{\text{Spec2}}, \tag{13}$$

where ϕ_{Tb} is described in (6). Note that satisfying φ_{Tbs} at time k means the train is starting to brake at time k. φ_{PBm} is True at time k when we allow the battery energy only to decrease (by forcing $P^-_B(k) = 0$ KW). Therefore, intuitively, φ_{Spec2} means that, if we anticipate the arrival of a braking train within the next 20 seconds (and if the supercapacitor's state is above the average reference value $E^r_S = 4.5$), we restrict the battery from increasing its energy level to pre-emptively create space for the rapid power surge. $\tilde{\varphi}_{\text{Spec2}}$ enforces φ_{Spec2} for all the prediction steps till $N_p - 1$.

3.4 ***Spec 3:*** *Safety of the Supercapacitor*

The third specification **Spec 3** concerns the supercapacitor. Unlike **Spec 1** and **Spec 2**, which rely on estimation data spanning the horizon N_e, this specification is independent of the train estimation. It aims to enhance the supercapacitor's ability to respond to real-time disturbances by ensuring sufficient flexibility in its energy level. This flexibility allows the supercapacitor to absorb or provide power as needed, ultimately enhancing the microgrid's resilience. We employ STL specifications for the safety objective due to their ability to incorporate temporal constraints in a specific manner, making the system safer without introducing excessive conservatism.

Concretely, we define a secure operating range by defining the energy window $E_S \in [\tilde{E}^m_S, \tilde{E}^M_S]$, with $E^m_S < \tilde{E}^m_S < \tilde{E}^M_S < E^M_S$. While $E_S(k)$ is permitted to violate this range temporarily, it is mandatory to return within it after a specific time (5 seconds) beyond the horizon N_p, which can be written as φ_{Spec3} in the following:

$$\varphi_{\text{Smax}} = [E_S(k) - \tilde{E}^M_S \leq 0], \tag{14}$$

$$\varphi_{\text{Smin}} = [\tilde{E}^m_S - E_S(k) \leq 0], \tag{15}$$

$$\varphi_{\text{Spec3}} = [\Diamond_{[0,5]}(\varphi_{\text{Smax}} \wedge \varphi_{\text{Smin}})], \tag{16}$$

$$\tilde{\varphi}_{\text{Spec3}} = \Box_{[-N_p+1,N_p-1]} \varphi_{\text{Spec3}}, \tag{17}$$

where satisfying the two specifications $\phi_{\text{Smax}} \wedge \phi_{\text{Smin}}$ means that the supercapacitor is in the secure operating range $E_S \in [\tilde{E}^m_S, \tilde{E}^M_S]$. Note that φ_{Spec3} allows to escape from this secured region up to four consecutive steps.

While we enforced $\Box_{[0,N_p-1]}$ for **Spec 1** and **Spec 2**, for **Spec 3** the horizon must also account for the fulfillment of φ within the *past* N_p-length trajectory. This means we impose $\Box_{[-N_p+1,N_p-1]}\varphi_{\text{Spec3}}$. This is crucial to satisfy the formula in the actual trajectory, not just in the predicted trajectory. The feasibility of **Spec 1** and **Spec 2** at each step is not dependent on the previous step; therefore, we need not consider this.

3.5 Optimal Control Problem

A receding horizon controller is built upon the control strategies in **Spec 1**–**3**. Given a time horizon N_p, the optimization problem we solve at each iteration is

$$\begin{aligned}
\mathcal{O} = \underset{\{u(k),\ldots,u(k)\}}{\text{argmin}} \quad & J(k) \\
s.t.\ & x(k+1) = Ax(k) + Bu(k) + Dd(k), \forall k \in [0, N_p - 1], \\
& \text{Constraints in Subsection 2.2 (e.g. (2), (3), (4)),} \\
& \tilde{\varphi}_{\text{Spec1}} \wedge \tilde{\varphi}_{\text{Spec2}} \wedge \tilde{\varphi}_{\text{Spec3}},
\end{aligned}$$

where $\tilde{\varphi}_{\text{Spec1}}$, $\tilde{\varphi}_{\text{Spec2}}$ and $\tilde{\varphi}_{\text{Spec3}}$ are the specifications in (9), (13) and (17), respectively. These STL specifications are transformed into constraints using a popular MILP encoding framework, as in Belta and Sadraddini (2019).

4. SIMULATIONS

We provide numerical results of the optimization problem $\mathcal{O}$ in the receding horizon approach. Unless otherwise noted, all parameter settings for the maximum/minimum limits of the state and control constraints are the same as the ones in Sheng et al. (2019). The simulation time is 160 s, with a sampling time of 1 s. The simulations are performed on a MacBook Air 2020 with an Apple M1 processor (Maximum CPU clock rate: 3.2 GHz) and 8GB of RAM. The computational time of the optimization problem at each iteration is less than one second for horizon $N_p = 10, N_e = 20$ even with the MIP-based solver, while we also found that increasing the prediction horizon N_p (e.g., $N_p = 40$) drastically increase computational time due to the nature of the MIP-based solver. We assume that the estimated data $\tilde{\boldsymbol{d}}$ is provided as:

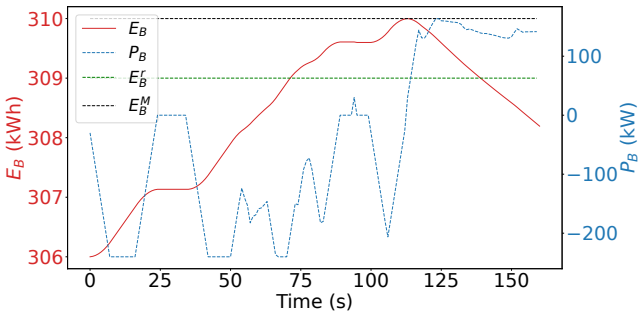

Fig. 2. $E_B = E_B^+ - E_B^-$ and $P_B = P_B^+ - P_B^-$

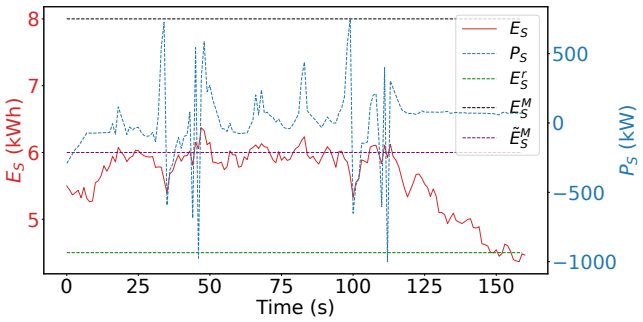

Fig. 3. $E_S = E_S^+ - E_S^-$ and $P_S = P_S^+ - P_S^-$

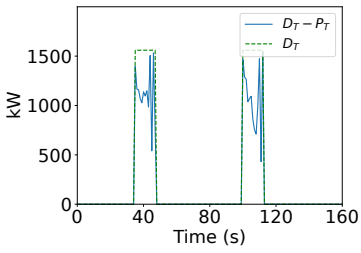

Fig. 4. $P_T = P_T^+ - P_T^-$

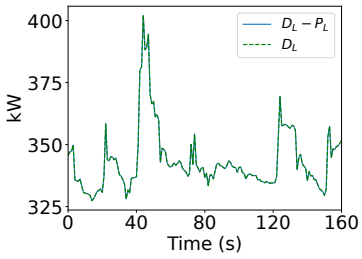

Fig. 5. $D_L - P_L$

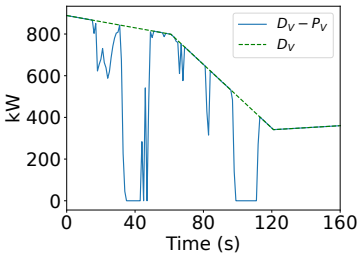

Fig. 6. $D_{PV} - P_{PV}$

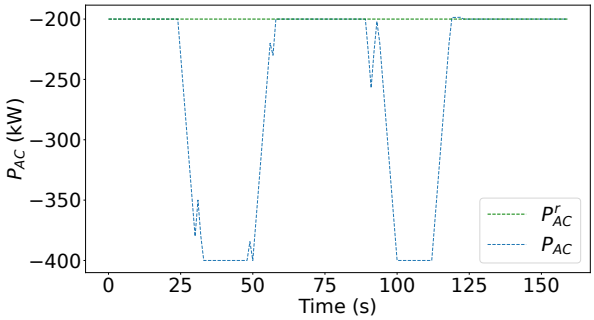

Fig. 7. $P_{AC} = P_{AC}^+ - P_{AC}^-$

$$\widetilde{\boldsymbol{d}} = \big([D_{PV}(0)\ D_L(0)\ D_T(0)]^\top, \ldots, [D_{PV}(0)\ D_L(N_p-1)\ D_T(N_p-1)]^\top \big), \tag{18}$$

where D_{PV} is unknown (and thus assumed constant $D_{PV}(0)$ throughout the horizon), while D_L and D_T are fully known within the horizon. Note that enhancements of the assumption on $\widetilde{\boldsymbol{d}}$ in (18) are possible, such as incorporating sensor data to improve the estimation of D_{PV} and incorporating uncertainties in D_L and D_T for horizons further into the future.

Figs. 2–7 show the satisfactory results of the suggested approach. Indeed, the microgrid can recover the most part of the regenerative braking energy (see Fig. 4) while not curtailing the load (see Fig. 5) and not violating the physical constraints. Furthermore, the whole set of specifications is respected, encompassing those formulated through the traditional cost function and those precisely defined through STL.

Regarding **Spec 1** on the power to the AC grid, Fig. 7 shows that the controller takes a value that is different from the reference of -200 KW only when we estimate that the train is going to brake in the next 10 seconds, that is, timespan $t \in [25, 58]$ and $t \in [90, 123]$ in this case. Due to the limitations on controllable power, the controller is restricted to operate only within these specific time intervals. Despite the loss of power from both the train and PV, the proposed controller remains feasible. It is important to note that, while this strategy of constraining PV power may result in a suboptimal solution, it aligns with the higher-level strategy decided at the tertiary layer, providing momentary benefits. Because of this restriction on the transmittable power on the control action, it cannot take any action outside of these timespans. Nevertheless, the control problem did not become infeasible while sacrificing the power from the train and the PV. It is worth mentioning that although this strategy of restricting the PV power makes the solution more restrictive, we enjoy the monetary benefits of this strategy decided on the higher tertiary layer.

Regarding **Spec 2**, Fig. 2 demonstrates the controller's strategic decision to halt battery charging before train arrivals (specifically during $t \in [25, 35]$ and $t \in [90, 100]$). This prevents the supercapacitor from hitting its maximum limit of 310 KWh for extended periods, except briefly at timestep 110 after the second train arrival. As seen in Fig. 7, during the interval between train brakings ($t \in [58, 90]$), **Spec 1** prevents power transfer to the AC grid ($P_{AC}^+ = 0.0$ KW). This poses a potential risk, as excess PV power could make the optimization problem infeasible. Importantly, **Spec 2** mitigates this risk – without it, the energy limit would be reached during this interval, leading to a higher infeasibility rate.

Regarding **Spec 3** on the supercapacitor, Fig. 3 shows that the controller consistently operates within the safe set $[\tilde{E}_S^m, \tilde{E}_S^M] = [3.0, 6.0]$ deviating from this range only when necessary. Notably, the controller reaches around 6.5 only during the train's arrival. Subsequently, without additional

power to manage, it returns to the reference value by the end of the simulation.

5. CONCLUSIONS

This paper demonstrates how to formally define complex temporal specifications and integrate them within a receding horizon optimization problem for managing power within a microgrid composed of diverse components. Future work aims to expand this approach into a unified framework capable of negotiating interactions across hierarchical control layers upon the principles established in this paper.

REFERENCES

Araúz, J. and Martinez, S. (2023). Methodology for assessing the impact of regenerative braking energy injection of a direct current railway system on the distribution grid. *Electric Power Systems Research*, 220, 109368.

Baier, C. and Katoen, J.P. (2008). *Principles of Model Checking*. MIT Press.

Beg, O.A., Nguyen, L.V., Johnson, T.T., and Davoudi, A. (2019). Signal temporal logic-based attack detection in dc microgrids. *IEEE Transactions on Smart Grid*, 10(4), 3585–3595. doi:10.1109/TSG.2018.2832544.

Belta, C. and Sadraddini, S. (2019). Formal methods for control synthesis: An optimization perspective. *Annual Review of Control, Robotics, and Autonomous Systems*, 2, 115–140.

Derler, P., Lee, E.A., and Sangiovanni Vincentelli, A. (2012). Modeling cyber–physical systems. *Proceedings of the IEEE*, 100(1), 13–28.

Donzé, A. and Raman, V. (2015). Blustl: Controller synthesis from signal temporal logic specifications. In G. Frehse and M. Althoff (eds.), *ARCH14-15. 1st and 2nd International Workshop on Applied veRification for Continuous and Hybrid Systems*, volume 34 of *EPiC Series in Computing*, 160–168. EasyChair.

Fainekos, G.E. and Pappas, G.J. (2009). Robustness of temporal logic specifications for continuous-time signals. *Theoretical Computer Science*, 410(42), 4262–4291.

Feng, C., Gao, Z., Sun, Y., and Chen, P. (2021). Electric railway smart microgrid system with integration of multiple energy systems and power-quality improvement. *Electric Power Systems Research*, 199, 107459.

González-Gil, A., Palacin, R., and Batty, P. (2013). Sustainable urban rail systems: Strategies and technologies for optimal management of regenerative braking energy. *Energy Conversion and Management*, 75, 374–388.

Iovine, A., Rigaut, T., Damm, G., De Santis, E., and Di Benedetto, M.D. (2019). Power management for a DC microgrid integrating renewables and storages. *Control Engineering Practice*, 85, 59–79.

Kurtz, V. and Lin, H. (2022). Mixed-integer programming for signal temporal logic with fewer binary variables. *IEEE Control Systems Letters*, 6, 2635–2640.

Liu, S., Saoud, A., Jagtap, P., Dimarogonas, D.V., and Zamani, M. (2022). Compositional synthesis of signal temporal logic tasks via assume-guarantee contracts. In *2022 IEEE 61st Conference on Decision and Control (CDC)*, 2184–2189.

Nuzzo, P., Xu, H., Ozay, N., Finn, J.B., Sangiovanni-Vincentelli, A.L., Murray, R.M., Donzé, A., and Seshia, S.A. (2014). A contract-based methodology for aircraft electric power system design. *IEEE Access*, 2, 1–25.

Parisio, A., Rikos, E., and Glielmo, L. (2014). A model predictive control approach to microgrid operation optimization. *IEEE Transactions on Control Systems Technology*, 22(5), 1813–1827.

Park, B. and Olama, M.M. (2021). Mitigation of motor stalling and fidvr via energy storage systems with signal temporal logic. *IEEE Transactions on Power Systems*, 36(2), 1164–1174.

Perez, F., Iovine, A., Damm, G., Galai-Dol, L., and Ribeiro, P.F. (2020). Stability analysis of a dc microgrid for a smart railway station integrating renewable sources. *IEEE Transactions on Control Systems Technology*, 28(5), 1802–1816.

Pham, T.H., Iovine, A., Olaru, S., Maeght, J., Panciatici, P., and Ruiz, M. (2022). Advanced management of network overload in areas with Renewable Energies Sources. In *11th Symposium on Control of Power and Energy Systems (CPES)*, volume 55, 81–86.

Raman, V., Donzé, A., Maasoumy, M., Murray, R.M., Sangiovanni-Vincentelli, A., and Seshia, S.A. (2014). Model predictive control with signal temporal logic specifications. In *53rd IEEE Conference on Decision and Control*, 81–87.

Scheepmaker, G.M. and Goverde, R.M. (2020). Energy-efficient train control using nonlinear bounded regenerative braking. *Transportation Research Part C: Emerging Technologies*, 121, 102852.

Sheng, Z., Iovine, A., Damm, G., and Galai-Dol, L. (2019). Power management for a dc microgrid in a smart railway station including recovery braking. In *2019 18th European Control Conference (ECC)*, 1418–1423.

Takayama, Y., Hashimoto, K., and Ohtsuka, T. (2023a). Signal temporal logic meets convex-concave programming: A structure-exploiting SQP algorithm for STL specifications. *in IEEE Conference on Decision and Control (CDC)*.

Takayama, Y., Hashimoto, K., and Ohtsuka, T. (2023b). STLCCP: An efficient convex optimization-based framework for signal temporal logic specifications. Preprint available at `https://arxiv.org/abs/2305.09441`.

Taousser, F.Z., Olama, M.M., Djouadi, S.M., Tomsovic, K., Zhang, Y., and Xue, Y. (2020). Model predictive control for voltage restoration in microgrids using temporal logic specifications. *IET Energy Systems Integration*, 2(3), 207 – 214.

Wooding, B., Vahidinasab, V., and Soudjani, S. (2020). Formal controller synthesis for frequency regulation utilising electric vehicles. In *International Conference on Smart Energy Systems and Technologies (SEST)*, 1–6.

Xu, Z., Julius, A., and Chow, J.H. (2018). Coordinated control of wind turbine generator and energy storage system for frequency regulation under temporal logic specifications. In *2018 Annual American Control Conference (ACC)*, 1580–1585.

Xu, Z., Julius, A., and Chow, J.H. (2019). Energy storage controller synthesis for power systems with temporal logic specifications. *IEEE Systems Journal*, 13(1), 748–759.